Available online at www.sciencedirect.com
SCIENCE DIRECT®
International Journal of Heat and Mass Transfer 48 (2005) 477–486
International Journal of HEAT and MASS TRANSFER
www.elsevier.com/locate/ijhmt

Numerical modeling of unidirectional stratified flow with and without phase change

Y.F. Yap, J.C. Chai *, K.C. Toh, T.N. Wong, Y.C. Lam

School of Mechanical and Production Engineering, Nanyang Technological University, Nanyang Avenue, Singapore 639798

Received 13 May 2004; received in revised form 10 September 2004
Available online 11 November 2004

Abstract

This article presents a mass correction procedure for unidirectional stratified flow of two fluids (or two phases of the same fluid) using the level-set method. A localized mass correction term is introduced to ensure mass conservation at every axial cross-section. The mass correction term is based on the mass flowrates. Phase change is captured using the mass correction term. For demonstration purposes, this article assumes that both phases are at their respective saturated states and the heat addition results in phase change at the saturation temperature. Results for various combinations of density, viscosity and mass flowrate ratios are presented. The proposed procedure is validated using available fully developed exact solutions for unidirectional stratified flow. The evolutions of the interface in the developing region are also captured and compares well with "exact" solutions.

1. Introduction

Two-phase flows are encountered in a variety of engineering applications. These include, but are not limited to, flow of polymers, and gas bubbles in liquids. There are two general types of two-phase flow prediction procedures [1]. These are the particle tracking method and the interpenetrating continua method. The particle tracking method is developed primarily to compute flows where the secondary phase travels along trajectories. In this situation, the primary phase is treated as a single phase. The resultant velocity field carries the secondary phase in the flow domain. If needed, the secondary phase can impart (usually localized) momentum source or sink on the primary phase. The other class of procedure can handle situations where both phases interact and affect each other significantly. These include, but are not limited to, the two-fluid model with IPSA [2], the height-of-liquid method [3], the volume-of-fluid (VOF) method [4] and the level-set (LS) method [5].

Recently, the LS method has been used to model (1) evolutions of bubbles under gravitational effect [6–9], (2) evolutions of bubbles carried by a primary fluid in pipes [10,11], (3) boiling and phase change [12–16], (4) thermocapillary pumping for electronic packaging [17], (5) moving solids [18] and (5) injection molding [19].

One drawback of the LS method is the loss (or gain) of mass. Various mass correction terms have been presented to overcome this shortcoming [7–9]. These procedures ensure *global* mass conservation of the two phases.

This article presents a mass correction scheme which ensures mass conservation at every cross-section along the flow direction for a unidirectional flow. Unlike the existing mass correction schemes, it is based on the *mass*

* Corresponding author. Tel.: +65 6790 4270; fax: +65 6792 4062.
E-mail address: mckchai@ntu.edu.sg (J.C. Chai).

0017-9310/$ - see front matter © 2004 Elsevier Ltd. All rights reserved.
doi:10.1016/j.ijheatmasstransfer.2004.09.017

Nomenclature

h_{fg}	latent heat of vaporization	x	coordinates
D	Dirac delta function	$\vec{x}$	position vector
H	Heaviside function	α	property
L	length	δ	interface location
$\dot{m}_c$	current mass flowrate	ε	grid size related parameter
$\dot{m}_{cor}$	mass preservation factor	Γ	diffusion coefficient
$\dot{m}_d$	desired mass flowrate	μ	viscosity
$\dot{m}_{evp}$	evaporation mass flowrate	ϕ	dependent variable
$\dot{m}''_{pc}$	mass flux due to phase change	ρ	density
p	pressure	ξ, ψ, ψ'	level-set functions
q	heat flux		
Q	total rate of heat addition	*Subscripts*	
S	source term	fd	fully developed
$t', \bar{t}$	pseudo-times	int	interface
u	velocity	liq	liquid
$\dot{V}$	volumetric flowrate	ref	reference phase
W	height	vap	vapor

flowrates. The analysis focuses on *steady-state* solutions of the continuity and momentum equations.

The remainder of this article is divided into three sections. The governing equations, the basis of the mass preservation scheme and the solution procedure are discussed in the next section. This is followed by the presentation of the results. Finally, some concluding remarks are given.

2. Mathematical formulation

2.1. Governing equations

The steady, incompressible continuity and momentum equations in Cartesian tensor notation for a two-phase flow problem can be written as

$$\frac{\partial u_j}{\partial x_j} = \left(\frac{1}{\rho_{vap}} - \frac{1}{\rho_{liq}}\right) \int \dot{m}''_{pc} D(\vec{x} - \vec{x}_{int})\, ds \tag{1}$$

$$\rho u_j \frac{\partial u_i}{\partial x_j} = \frac{\partial}{\partial x_j}\left(\mu \frac{\partial u_i}{\partial x_j}\right) - \frac{\partial p}{\partial x_i} + \frac{\partial}{\partial x_j}\left(\mu \frac{\partial u_j}{\partial x_i}\right) \tag{2}$$

where ρ, μ, $\dot{m}''_{pc}$, D, $\vec{x}$, $\vec{x}_{int}$ and ds are the density and the viscosity appropriate for the phase occupying the particular spatial location, the mass flux due to phase change, the Dirac delta function, the position vector, the position vector of the interface and the infinitesimal area of the interface, respectively. The source term in Eq. (1) accounts for the density difference in the liquid–vapor phase change effect. In this article, the capillary number is assumed to be large. As a result, the surface tension term is not included in Eq. (2). The mass correction scheme can be used even when the surface tension term is included. The density and viscosity are calculated using

$$\alpha = (1 - H)\alpha_1 + H\alpha_2 \tag{3}$$

In Eq. (3), α can be the density or viscosity. The Heaviside function H is related to the normal distance from the interface and is calculated using [7]

$$H = \begin{cases} 0 & \xi < -\varepsilon \\ \dfrac{\xi + \varepsilon}{2\varepsilon} + \dfrac{1}{2\pi}\sin\left(\dfrac{\pi\xi}{\varepsilon}\right) & |\xi| \leqslant \varepsilon \\ 1 & \xi > \varepsilon \end{cases} \tag{4}$$

In Eq. (4), ε is related to the grid size and is usually taken as a factor of the grid spacing. In this combined formulation, an additional scalar variable, called the level-set function, is used to identify the distances from the interface between the two phases and the reference plane. The equation governing the evolution of the level-set function is

$$u_j \frac{\partial \xi}{\partial x_j} = \frac{\dot{m}''_{pc}}{\rho} |\nabla \xi| \tag{5}$$

In Eq. (5), the mass flux due to phase change $\dot{m}''_{pc}$, is zero when there is no phase change. In the proposed approach, Eq. (5) without the mass flux term is solved. This is written as

$$u_j \frac{\partial \xi}{\partial x_j} = 0 \tag{6}$$

In the absence of phase change Eq. (6) is sufficient to capture the evolution of the distance function. However, mass of the various "phases" might not be conserved. As a result, a mass correction step is introduced to ensure mass conservation. With phase change, in addition to the above-discussed mass "error", Eq. (6) introduces an additional error due to the omission of the phase change mass flux. As a result, in problems with phase change, the mass correction step is used to account for the mass flux due to phase change and the mass "error" due to the inability of the level-set method to conserve mass. Details of this mass correction step will be discussed later.

In the solution of the level-set function (Eq. (6)), any convenient reference value can be assigned to the interface. The values of ξ at all node points are then calculated based on the reference value at the interface. The level-set function ξ, is the *normal* distance from the interface. It is therefore a distance function which satisfies $|\nabla\xi| = 1$. The value of ξ at the interface is set to zero. As a result, ξ has opposite signs in the two phases. For this formulation to work properly, ξ must remain a distance function. However, this can only be ensured at the beginning of the iteration process where the location of the interface is assumed and the values of ξ at all nodes are specified. During the iteration process, the values of ξ are calculated using Eq. (6). Although the interface is still represented by the reference value, the other values of ξ might not be the distances from the interface. As a result, another scalar variable is defined and solved. This variable must be a distance function and has the same interface value as ξ. The "steady-state" solution of ψ given in Eq. (7) satisfies the above requirements.

$$\frac{\partial\psi}{\partial\bar{t}} = \mathrm{sign}(\xi)(1 - |\nabla\psi|) \tag{7}$$

In Eq. (7), $\bar{t}$ is a pseudo-time for the variable ψ. Eq. (7) is subjected to the following initial condition.

$$\psi(\vec{x}, 0) = \xi(\vec{x}) \tag{8}$$

It is clear from Eq. (7) that the "steady-state" solution satisfies $|\nabla\psi| = 1$. Thus, it is a distance function. The initial value (Eq. (8)) ensures that the interface value of ψ is identical to the interface value of ξ. As a result, the "steady-state" values of ψ are the distances from the interface. Although Eq. (7) ensures ψ and thus ξ as the distance function, it suffers a significant drawback. It does not ensure the conservation of mass of the various phases. To ensure mass conservation at each cross-section of a unidirectional flow, a local mass correction factor is defined and an additional equation is solved. This is written as

$$\frac{\partial\psi'}{\partial t'} = \dot{m}_{\mathrm{cor}} \tag{9}$$

In Eq. (9), t' and $\dot{m}_{\mathrm{cor}}$ are pseudo-time (which can be different from the pseudo-time $\bar{t}$) and mass conservation factor, respectively. For the unidirectional flow without phase change (Fig. 1), the *mass flowrate* at every axial location remains constant. As a result, Eq. (9) must be ensured at every axial cross section. The local mass correction factor is

$$\dot{m}_{\mathrm{cor}} = \mathrm{sign}(\xi_{\mathrm{ref}})\frac{(\dot{m}_{\mathrm{d}} - \dot{m}_{\mathrm{c}})}{\dot{m}_{\mathrm{d}}} \tag{10}$$

where $\dot{m}_{\mathrm{d}}$ and $\dot{m}_{\mathrm{c}}$ are the desired mass flowrate and the most current local mass flowrate of the reference phase, respectively. Depending on the choice of the Heaviside function of the reference phase, the mass flowrate of the reference phase can be calculated using

$$\dot{m} = \begin{cases} \sum \rho_{\mathrm{ref}} Hu\Delta A & H_{\mathrm{ref}} = 1 \\ \sum \rho_{\mathrm{ref}}(1-H)u\Delta A & H_{\mathrm{ref}} = 0 \end{cases} \tag{11}$$

The summation is performed over a cross-section. In the absence of phase change, the desired mass flowrate is calculated using the *inlet* condition. This mass correction scheme is also used to account for phase changes due to evaporation or condensation. For such situations, the desired mass flowrate is calculated from the conservation of mass over a control volume. Fig. 2 shows a situation where heat is added to the channel and the liquid phase is transformed into vapor through evaporation. When both phases are at their respective saturated states and the heat addition results in phase change, the total heat added (Fig. 2) is related to the evaporation mass flowrate through

$$\dot{m}_{\mathrm{evp}} = \frac{Q}{h_{fg}} \tag{12}$$

In Eq. (12), $\dot{m}_{\mathrm{evp}}$, Q and h_{fg} are the mass flowrate of the evaporated liquid phase, the total rate of heat addition and the latent heat of vaporization, respectively. The desired mass flowrate is related to known mass flowrate of an upstream location (Fig. 2) and can be written as

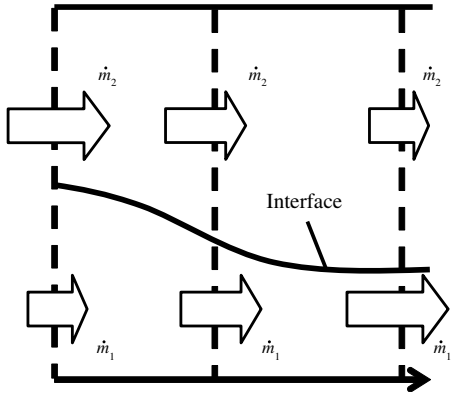

Fig. 1. Mass flowrates at three axial locations.

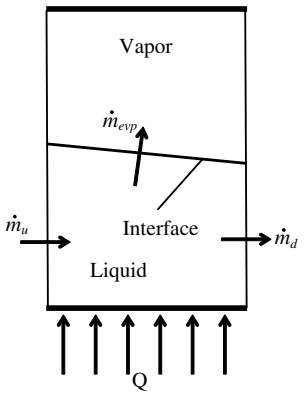

Fig. 2. Conservation of mass during evaporation.

$$\dot{m}_{\mathrm{d}} = \dot{m}_{\mathrm{u}} - \dot{m}_{\mathrm{evp}} \tag{13}$$

In Eq. (13), $\dot{m}_{\mathrm{u}}$ is the known mass flowrate of an upstream location. Eqs. (12) and (13) can be used to model condensation. In such situation, heat is being removed from the channel and thus the heat transfer rate Q will be negative.

In non-isothermal situations, the energy equation must be solved. Eq. (12) must be modified to include the temperature gradient at the interface and the energy convected into and out of the control volume shown in Fig. 2.

2.2. Summary of the solution procedure

The solution procedure can be summarized as follows:

1. Guess the locations of the interface.
2. Calculate the normal distances for all nodes from the interface.
3. Specify the properties for all nodes using Eqs. (3) and (4).
4. Solve the continuity and momentum equations given by Eqs. (1) and (2).
5. Solve for ξ (Eq. (6)) using the velocities obtained in Step 4.
6. Solve for the "steady-state" ψ (Eq. (7)) using the values of ξ from Step 5 as the initial values.
7. Solve for the "steady-state" ψ' (Eq. (9)) using the values of ψ from Step 6 as the initial values.
8. Set $\xi(\vec{x}) = \psi'(\vec{x})$.
9. Repeat Steps 3 through 8 until the solution converges.

At the end of the first "steady-state" solution (Step 6), ψ is a distance function. However, mass might not be conserved. The "steady-state" solution at the end of Step 7 ensures that ψ' is a distance function and also conserves mass.

2.3. Numerical method

The continuity equation (Eq. (1)), momentum equation (Eq. (2)), the level-set equations (Eqs. (6), (7) and (9)) are special cases of a general transport equation

$$\rho\frac{\partial\phi}{\partial t} + \rho u_j\frac{\partial\phi}{\partial x_j} = \frac{\partial}{\partial x_j}\left(\Gamma\frac{\partial\phi}{\partial x_j}\right) + S \tag{14}$$

where ϕ, ρ, Γ, and S are the dependent variables, density, diffusion coefficient and source term, respectively. The finite-volume method of Patankar [20] is used to solve the transport equation given in Eq. (14). A staggered grid is used in this article. The scalar variables are stored at the centers of the control volumes, while the velocities are located at the control volume faces. In this article, the power-law of [20] is used to model the combined convection–diffusion effect in the momentum equations. The first-order upwind scheme is used to model the convection of the level-set equations. The SIMPLER algorithm is used to resolve the velocity-pressure coupling. The fully implicit scheme is used to discretize the transient term. The resulting algebraic equations are solved using the TriDiagonal Matrix Algorithm.

The first level-set equation (Eq. (6)) is the "steady-state" form of Eq. (14) with $\rho = 1$, $\Gamma = 0$ and $S = 0$. The second level-set equation (Eq. (7)) is modeled using $\rho = 1$, $u = v = 0$, $\Gamma = 0$ and $S = \mathrm{sign}(\psi)(1 - |\nabla\psi|)$. The mass preservation equation (Eq. (9)) is modeled using $\rho = 1$, $u = v = 0$, $\Gamma = 0$ and $S = \dot{m}_{\mathrm{cor}}$.

3. Results and discussions

Fig. 3 shows the schematic of the problems considered in this article. Two immiscible fluids (or two phases of the same fluid) flow a distance L between two parallel plates separated by a distance W. For a given set of density ratio, and mass flowrate ratio, the inlet "thickness" δ_{in} of fluid 1 determines the inlet velocities of both fluids namely, $u_{\mathrm{in},1}$ and $u_{\mathrm{in},2}$. As the flow develops, the velocity

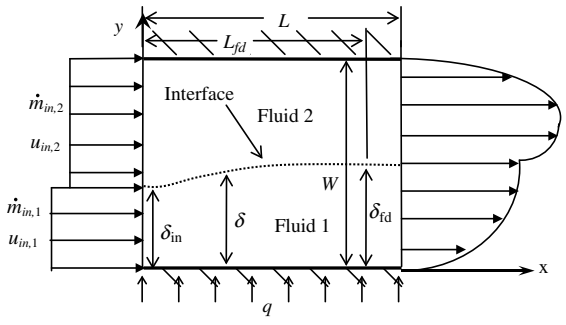

Fig. 3. Flow of two immiscible fluids (or two phases of the same fluid) between parallel plates.

profile at every section changes along the axial direction. As a result, the interface δ between the two fluids evolves along the flow direction. Once the fully developed region is reached, the velocity profile and the interface location δ become independent of the axial coordinate.

Three problems are considered in this article. In the first problem, the densities and viscosities of the two fluids are set to the same values. The second problem shows the capabilities of the procedure in capturing the flows of two immiscible fluids of different densities and viscosities. The third problem demonstrates the capability of the proposed formulation in modeling phase change effects. Unless otherwise specified, the dimensionless velocity (u/u_{ave}) profiles are used in the following discussions.

3.1. Two immiscible fluids with same properties

In this problem, two immiscible fluids with the same densities $\rho_1 = \rho_2$ and the same viscosities $\mu_1 = \mu_2$ flow between two parallel plates. With this choice of properties, the fully developed velocity profile is that for a *single-fluid*.

To initiate this study, the inlet velocities of the two phases are also set to the same value namely, $u_{in,1} = u_{in,2} = u_{in}$. With this additional restriction, the velocity field in both the developing and fully developed regions are the same as the single-fluid velocity field. As an example, the inlet interface is located at $\delta_{in}/W = 0.3$. This implies a mass flowrate ratio of $\dot{m}_1/\dot{m}_2 = 3/7$. The inlet velocities of the two fluids are calculated based on the single fluid Reynolds number Re of 1. Using this Re, the inlet velocities are

$$u_{in,1} = u_{in,2} = u_{in} = \frac{\mu Re}{\rho W} \tag{15}$$

The length L and height W of the channel are set to 1 and 1, respectively. Zero axial gradient condition is used at the exit. The effects of grid resolutions on the interface evolutions with and without mass correction are shown in Fig. 4. Computations are carried out using 10×10, 20×20, 30×30, 40×40, and 50×50 uniformly spaced control volumes. It can be seen that the interface evolutions do not change when 40×40, and 50×50 control volumes are used. As a result, unless otherwise specified, all subsequent results are obtained using 40×40 control volumes.

Without mass correction, the fully developed interface locations vary with grid resolution before converging to its grid independent fully developed location. It is interesting to point out that with mass correction, the interface location in the fully developed region is the same irrespective of the number of control volumes used. For quantitative analysis, a term called the mass error is defined as

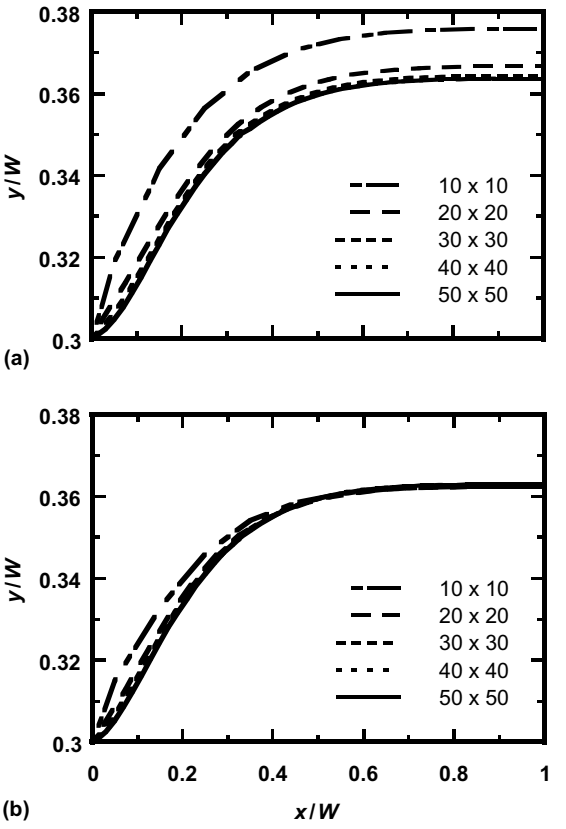

Fig. 4. Variation of δ/W along x/W for $\delta_{in}/W = 0.3$, $Re = 1$, $u_1 = u_2$, $\rho_1 = \rho_2$ and $\mu_1 = \mu_2$. (a) Without and (b) with mass correction.

$$\dot{m}_{ERR,k} \equiv \frac{|\dot{m}_{in,k} - \dot{m}_{cal,k}|}{\dot{m}_{in,k}} \tag{16}$$

In Eq. (16), $\dot{m}_{in,k}$ and $\dot{m}_{cal,k}$ are the inlet mass flowrate and the calculated (local) mass flowrate, respectively for fluid k. The mass errors for fluid k (Eq. (16)) are shown in Fig. 5. Without mass correction, the mass errors are finite. These mass errors reduce to machine zero (10^{-16}) with mass correction. For further comparisons, the interface locations along the axial locations are calculated and compared with the numerical predictions. The "exact" solutions are obtained by ensuring the conservation of mass of fluid 1 using the discrete local *single-fluid* velocity profile. For ease of discussion, assume the area occupied by fluid 1 spans from the first control volume to part of control volume N as shown in Fig. 6. The interface location δ is then

$$\delta = \sum_{j=1}^{N-1} \Delta y_j + f \Delta y_N \tag{17}$$

where f is the fraction of the area of control volume N occupied by fluid 1. The fraction f can be obtained

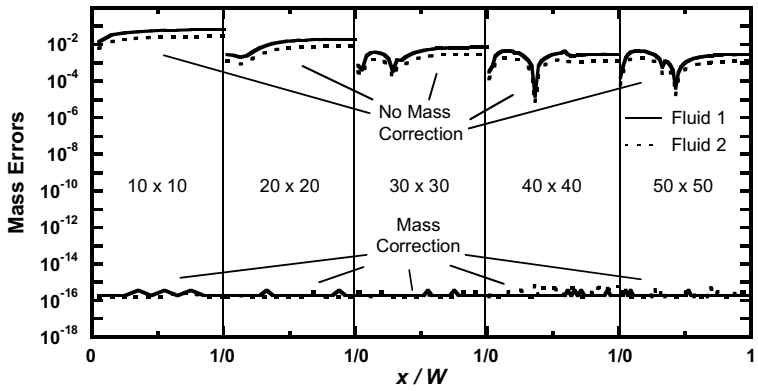

Fig. 5. Variation of mass error along x/W with and without mass correction.

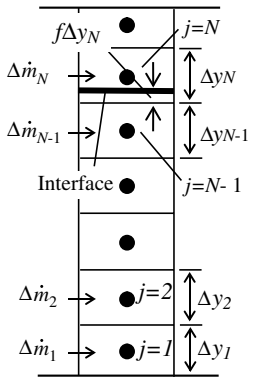

Fig. 6. Control volumes at a given axial section.

by ensuring the conservation of mass of fluid 1. Let the mass flowrate into control volume j at x be $\Delta\dot{m}_j$. Then, the mass flow rate of fluid 1 can be written as

$$\dot{m}_{\mathrm{in},1} = \sum_{j=1}^{N-1} \Delta\dot{m}_j + f\Delta\dot{m}_N \tag{18}$$

or

$$f = \frac{\dot{m}_{\mathrm{in},1} - \sum_{j=1}^{N-1} \Delta\dot{m}_j}{\Delta\dot{m}_N} \tag{19}$$

Fig. 7 shows the velocity profiles at six axial locations and the interface between the two fluids. These are obtained with mass correction. The fully developed velocity profile is identical to the exact solution from single fluid. The interface also agrees with the "exact" solution *exactly*. This problem shows that with mass correction, the interface evolution between two immiscible fluids is well captured.

Fig. 8 shows the ability of the procedure in predicting the evolution of the interface with non-uniform inlet velocity profile. Similar to the previous problem, the inlet interface is located also at $\delta_{\mathrm{in}}/W = 0.3$. The inlet Reynolds numbers (Eq. (20)) of fluid 1 and fluid 2 are

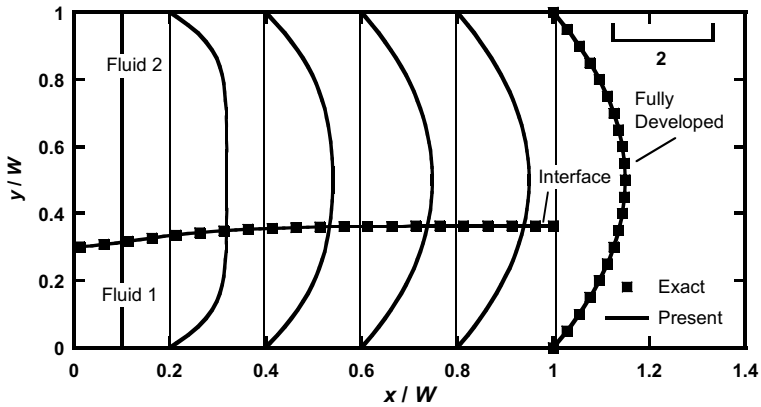

Fig. 7. Evolutions of velocity and interface profiles along x/W for $\delta_{\mathrm{in}}/W = 0.3$, $Re = 1$, $u_1 = u_2$, $\rho_1 = \rho_2$ and $\mu_1 = \mu_2$.

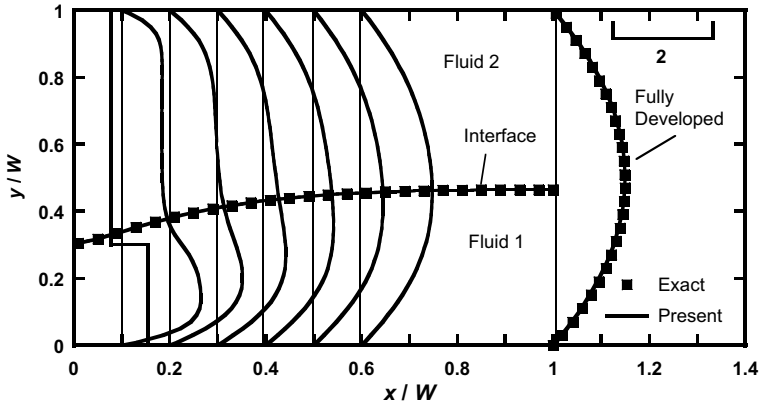

Fig. 8. Evolutions of velocity and interface profiles along x/W for $\delta_{in}/W = 0.3$, $Re_1 = 2Re_2 = 2$, $\rho_1 = \rho_2$ and $\mu_1 = \mu_2$.

set to 2 and 1, respectively. This results in a mass flowrate ratio of $\dot{m}_1/\dot{m}_2 = 6/7$.

$$Re = \frac{\rho u_{in} W}{\mu} \tag{20}$$

From Fig. 8, as expected, the single-fluid velocity profile is recovered in the fully developed region. The predicted interface compares well with the "exact" solution. Comparing Figs. 7 and 8, fluid 1 occupies more of the flow area when the inlet velocity is increased.

3.2. Two immiscible fluids with different properties

In this problem, the flow of two immiscible fluids of different densities, viscosities and inlet mass flowrates between two parallel plates is examined. For this type of problem, the fully developed velocity profile and interface location are functions of the viscosity ratio and the volumetric flowrate ratio and are independent of the inlet interface location [21,22]. Similar to the previous example, zero axial gradient condition is used at the exit. For demonstration purposes, a parallel plate channel with $L/W = 2$ is studied. The density ratio ρ_1/ρ_2, mass flowrate ratio $\dot{m}_1/\dot{m}_2$, viscosity ratio μ_1/μ_2 are taken as 2, 0.837, and 10, respectively. These values are chosen so that the interface is located at $y/W = 0.5$ in the fully developed region. A grid independent study shows that 40×40 uniformly spaced control volumes produces a grid independent solution. Fig. 9 shows the evolutions of the interface for three values of the inlet interface locations δ_{in}/W namely, 0.3, 0.5 and 0.7, respectively. As expected, the interfaces evolve along the axial direction. Downstream from the entrance, all interfaces reach their fully developed value of 0.5. It is interesting to note that the interface developed faster when $\delta_{in}/W = 0.7$ (than when $\delta_{in}/W = 0.3$). This will be explained later. Fig. 10 shows the evolutions of the

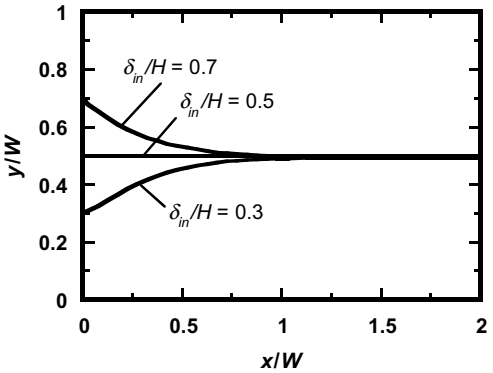

Fig. 9. Evolutions of δ/W along the axial direction for the flow of two-immiscible fluids between parallel plates for three inlet interface locations.

velocity fields and interfaces for δ_{in}/W of 0.3 and 0.7. Once the flow is fully developed, all velocity profiles settle to the same shape. The predicted fully developed velocity profiles compare very well with the exact solution [21]. Although not shown, the interface profiles in the developing region compare well with the "exact" solution given by Eq. (17). From Fig. 10, it can be seen that the inlet velocity profile with $\delta_{in}/W = 0.7$ is closer to the fully developed profile than the inlet velocity profile when $\delta_{in}/W = 0.3$. As a result, the interface developed faster when $\delta_{in}/W = 0.7$. Churchill [22] derived the fully developed interface thickness as function of the viscosity and volumetric flowrate ratios. Fig. 11 shows the comparisons between the present computations and the exact solutions [22]. It can be seen that the present procedure captures the interface locations correctly for the ranges of viscosity and volumetric flowrate ratios studied.

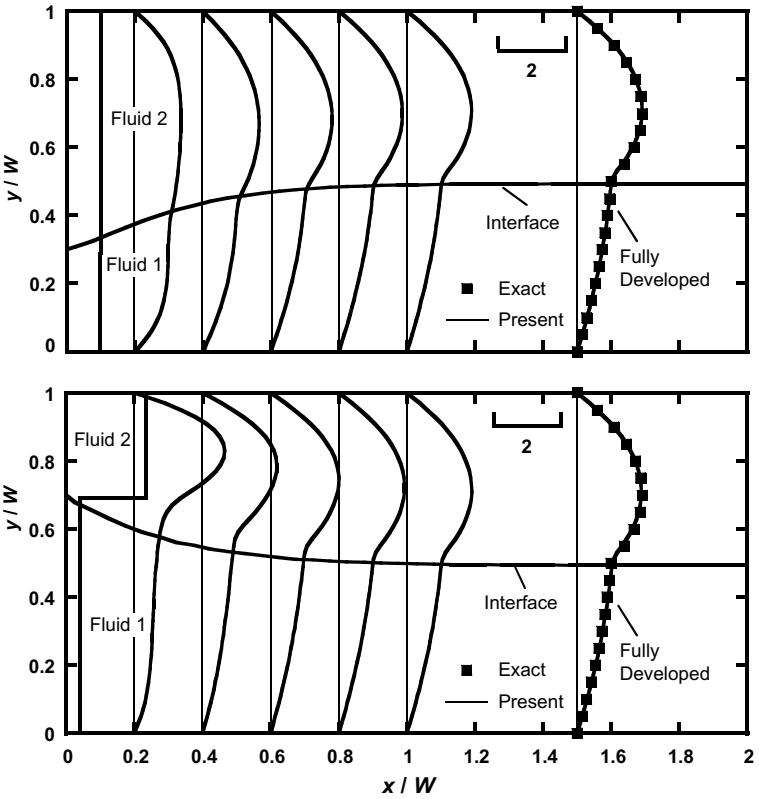

Fig. 10. Evolutions of velocity and interface profiles along the axial direction for the flow of two-immiscible fluids with $\rho_1/\rho_2 = 2$, $\dot{m}_1/\dot{m}_2 = 0.837$, $\mu_1/\mu_2 = 10$.

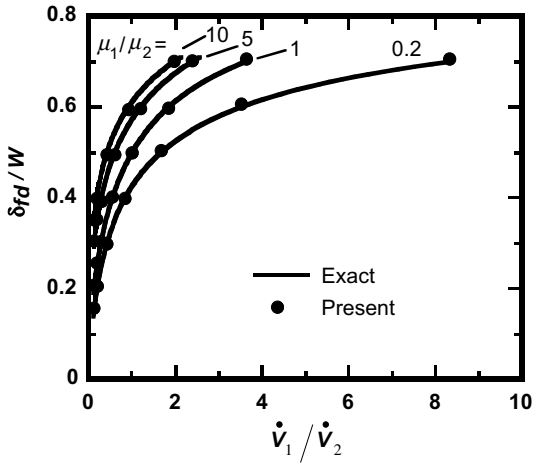

Fig. 11. Fully developed interface location δ_{fd}/W versus volumetric flow ratio $\dot{V}_1/\dot{V}_2$; comparisons of numerical and exact solutions.

3.3. Liquid–vapor flow with phase change

In this section, the interface development of liquid flow with vaporization due to heat addition is examined. The focus of this problem is on the prediction of the interface evolution in the presence of vaporization. The viscosities and inlet velocities of the two (liquid and vapor) phases are set to the same values. The density ratio ρ_{liq}/ρ_{vap} is set to 2. The inlet interface is set to $\delta_{in}/W = 0.3$ which implies a mass flowrate ratio $\dot{m}_{liq}/\dot{m}_{vap}$ of 6/7. The length to height ratio L/W is set to 2. The initial portion ($0 \leqslant x/W \leqslant 1$) of the channel

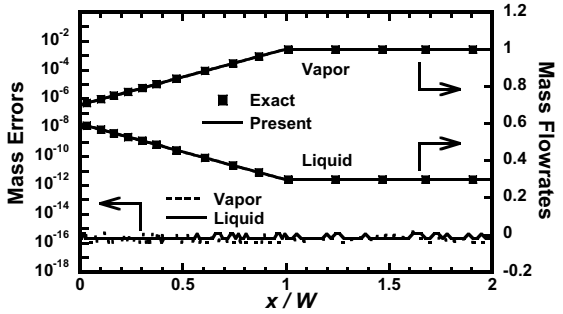

Fig. 12. Variation of mass flowrates and mass error along x/W for liquid–vapor flow with phase change.

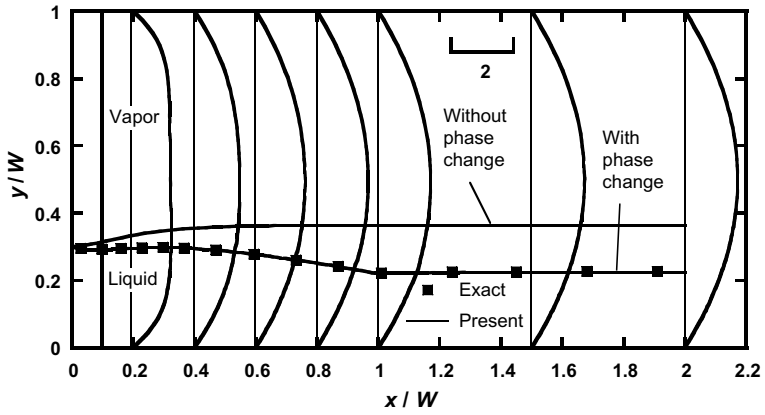

Fig. 13. Evolutions of velocity and interface profiles along the axial direction for liquid–vapor flow with phase change.

is heated while, the remaining of the channel walls is insulated. This can be written as

$$\dot{m}''_{\mathrm{pc}} = \begin{cases} 0.3 & 0 \leqslant x/W \leqslant 1 \\ 0 & 1 < x/W \leqslant 2 \end{cases} \tag{21}$$

Fig. 12 shows the mass flowrates and mass errors of the two phases as functions of the axial coordinate. As expected, the mass errors reduce to machine zero at all axial locations. In the initial portion of the channel, due to evaporation, the mass flowrate of the liquid phase decreases along the flow direction. The reverse is observed for the vapor phase. These mass flowarates become constant in the unheated portion of the channel. The liquid phase and vapor phase mass flowrates predicted using the proposed approach compare well with the exact solutions (Eq. (13)). Fig. 13 shows the interface evolutions along the axial coordinates. As expected, the liquid layer is thinner with evaporation. Again, the solution compares well with the exact solution.

4. Concluding remarks

A localized mass correction scheme for unidirectional stratified flow, which allows for phase change, is presented. The mass correction scheme is used to model flows between parallel plates with and without evaporation. Effects of density, viscosity and mass flowrate ratios are examined. Results arising from use of the proposed scheme compare very well with available exact solutions.

References

[1] S.V. Patankar, Review of Calculation Methods for Single-Phase and Multiphase Flows, UMSI report 92/53, 1992.

[2] D.B. Spalding, Numerical computation of multiphase flow and heat transfer, Recent Adv. Numer. Meth. Fluids 1 (1980) 139–168.

[3] B.D. Nichols, C.W. Hirt, Calculating three-dimensional free surface flows in the vicinity of submerged and exposed structures, J. Comput. Phys. 12 (1973) 234–246.

[4] C.W. Hirt, B.D. Nichols, Volume of fluid (VOF) methods for the dynamics of free boundaries, J. Comput. Phys. 39 (1981) 201–225.

[5] S. Osher, J.A. Sethian, Fronts propagating with curvature-dependent speed: algorithms based on Hamilton–Jacobi formulations, J. Comput. Phys. 79 (1988) 12–49.

[6] M. Sussman, P. Smereka, S. Osher, A level set approach for computing solutions to incompressible two-phase flow, J. Comput. Phys. 114 (1994) 146–159.

[7] Y.C. Chang, T.Y. Hou, B. Merriman, S. Osher, A level set formulation of eulerian interface capturing methods for incompressible fluid flows, J. Comput. Phys. 124 (1996) 449–464.

[8] H. Zhang, L.L. Zheng, V. Prasad, T.Y. Hou, A curvilinear level set formulation for highly deformable free surface problems with application to solidification, Numer. Heat Transfer B 34 (1998) 1–20.

[9] G. Son, A numerical method for incompressible two-phase flows with open or periodic boundaries, Numer. Heat Transfer B 39 (2001) 45–60.

[10] C. Kaliakatsos, S. Tsangaris, Motion of deformable drops in pipes and channels using Navier–Stokes equations, Int. J. Numer. Meth. Fluids 34 (2000) 609–626.

[11] M. Quecedo, M. Pastor, Application of the level set method to the finite element solution of two-phase flows, Int. J. Numer. Meth. Eng. 50 (2001) 645–663.

[12] G. Son, V.K. Dhir, Numerical simulation of film boiling near critical pressures with a level set method, J. Heat Transfer 120 (1998) 183–192.

[13] L.L. Zheng, H. Zhang, An adaptive level set method for moving-boundary problems: application to droplet spreading and solidification, Numer. Heat Transfer B 37 (2000) 437–454.

[14] D. Wheeler, C. Bailey, Modelling the melting and solidification of solder material, Adv. Electron. Packaging 1 (1999) 397–404.

[15] G. Son, A numerical method for bubble motion with phase change, Numer. Heat Transfer B 39 (2001) 509–523.
[16] F. Bazdidi-Tehrani, S. Zaman, Two-phase heat transfer on an isothermal vertical surface: a numerical simulation, Int. J. Heat Fluid Flow 23 (2002) 308–316.
[17] S.P. Gurrum, S. Murthy, Y.K. Joshi, Numerical simulation of thermocapillary pumping using level set method in: 5th ISHMT/ASME Heat and Mass Transfer Conference, January 3–5, Kolkata, India, 2002.
[18] M.H. Chung, A level set approach for computing solutions of inviscid compressible flow with moving solid boundary using fixed cartesian grids, Int. J. Numer. Meth. Fluids 36 (2001) 373–389.
[19] E.J. Holm, H.P. Langtangen, A unified finite element model for the injection molding process, Comput. Meth. Appl. Engrg. 178 (1999) 413–429.
[20] S.V. Patankar, Numerical Heat Transfer and Fluid Flow, Hemisphere Publisher, New York, 1980.
[21] R.B. Bird, W.E. Stewart, E.N. Lightfoot, Transport Phenomena, John Wiley & Sons Inc., New York, 1971.
[22] S.W. Churchill, Viscous Flows: The Practical Use of Theory, Butterworths Publishers, 1988.